TTP 95–16
hep-ph/9504345
April 1995

TESTING CP PROPERTIES OF HIGGS BOSONS *

M. L. STONG
Inst. Theor. Teilchenphysik, Universität Karlsruhe, Kaiserstraße 12
D-76128 Karlsruhe, Germany
E-mail: ml@ttpux6.physik.uni-karlsruhe.de

ABSTRACT

Possibilites for measuring the J^{PC} quantum numbers of the Higgs particle through its interactions with gauge bosons and with fermions are discussed. Observables which indicate CP violation in these couplings are also identified.

1. Introduction

While the Higgs particle in the Standard Model[1] must necessarily be a scalar state, assigned the external quantum numbers $J^{PC} = 0^{++}$, the Higgs spectrum in extended models such as supersymmetric theories may also include pseudoscalar ($J^{PC} = 0^{-+}$) states[2]. This assignment of the quantum numbers suggests the investigation of experimental opportunities to measure the parity of the Higgs states. The experimental observables useful in these measurements are also useful in studying the question of whether CP violation exists in the Higgs sector.

Several interesting methods exist to study these problems. The parity of the Higgs is reflected in the form of its coupling to fermion and to gauge-boson pairs, thus providing angular correlations in associated production of Higgs and one Z boson[3,4] as well as in the Higgs decays to gauge-boson[3,5] and fermion[6] pairs.

Another possibility is in the production of neutral Higgs particles in linearly-polarized photon–photon collisions[7]. The production of scalar particles requires parallel polarization of the two photons involved, whereas pseudoscalar particles require perpendicular polarization.

These Higgs production and decay mechanisms are discussed below. The generic notation H is used for the 0^{++} particles and A for the 0^{-+} states. When mixed states are considered, the notation ϕ is used.

2. Higgs Production in $e^+e^- \to Z\phi$.

We consider an effective lagrangian which contains the Standard Model couplings

*Invited Talk given at the Ringberg Workshop "Perspectives for Electroweak Interactions in e^+e^- Collisions," Munich, Feb. 5–8,1995.

of fermions to the Z and γ, and study the effects of the following ϕZZ couplings:

$$\mathcal{L}_{eff} = a_Z\,\phi Z^\mu Z_\mu + b_Z\,\phi Z^{\mu\nu}\widetilde{Z}_{\mu\nu} \tag{1}$$

where $Z_{\mu\nu} = \partial_\mu Z_\nu - \partial_\nu Z_\mu$, and $\widetilde{Z}_{\mu\nu} \equiv \frac{1}{2}\varepsilon_{\mu\nu\alpha\beta}V^{\alpha\beta}$, with the convention $\varepsilon_{0123} = +1$. The term a_Z has the form of the Standard Model ϕZZ coupling ($a_Z = g_Z m_Z/2$) and would correspond to a CP-even scalar ϕ, while the term b_Z corresponds to a CP-odd pseudoscalar ϕ. The presence of both terms indicates that ϕ is not a CP eigenstate. In the most general gauge-invariant dimension-six lagrangian[8,9], there would be additional CP-even terms. These have been neglected here under the assumption that they are suppressed two powers of some large energy scale relative to a_Z and appear only in interference terms with the above couplings.

The total cross section for $e^+e^- \to Z\phi$ contains no interference terms ($\sim a_Z b_Z$) and thus no observable CP violation. Figure 1 shows the change in the total cross section for this process for a small coupling b_Z in addition to the Standard Model a_Z. A forward-backward asymmetry in the Z scattering angle would be a signal for CP violation in this reaction. Such an asymmetry is not only CP-odd but also CP$\widetilde{\mathrm{T}}$-odd[10], and hence is proportional to the Z width in the approximation of neglecting imaginary parts in the effective couplings. Such an asymmetry occurs when one includes $\phi Z\gamma$ couplings in the lagrangian (1). Transverse polarization of the electron beams does not provide additional information for this reaction, whereas longitudinal polarization is useful for studying the $\phi Z\gamma$ CP-even couplings[4].

Fig. 1. Cross section for $e^+e^- \to ZH$, for $(\sqrt{s}, m_H) = (200{,}60)$ and $(300{,}150)$ GeV. The horizontal solid lines give the Standard Model values and the dotdashed curves show the dependence on b_Z.

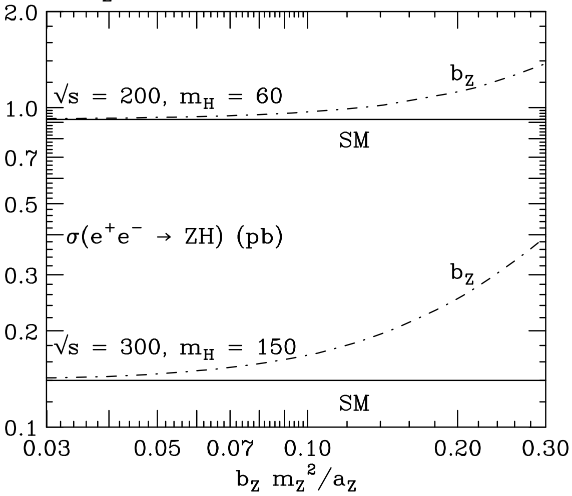

Fig. 2. Differential cross sections (separately normalized) for $e^+e^- \to ZH$, (ZA, ZZ), with $(\sqrt{s}, M_H) = (500{,}100)$ GeV. The solid (dotdashed,dashed) line indicates the ZH (ZA,ZZ) cross section.

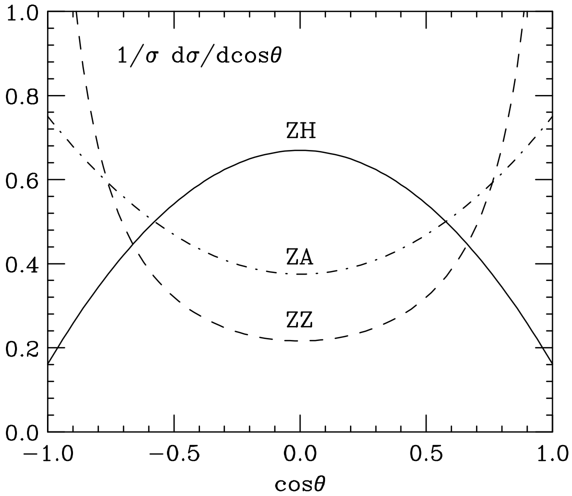

The two types of terms given here have rather different characteristics[3]. The CP-even term a_Z is an S-wave coupling of the ϕ to the Z's. The Z bosons produced are a mixture of longitudinal and transverse polarization states. In the high-energy limit, the mixture becomes purely longitudinal, and the angular distribution in the Z scattering angle relative to the electron has the form $d\sigma/d\cos\theta \propto \sin^2\theta$. The CP-odd coupling b_Z is a P-wave coupling and the produced Z bosons are purely transversally polarized for any energy, so that $d\sigma/d\cos\theta \propto 1-\sin^2\theta/2$.

Although CP violation may be difficult to observe in this reaction, the identification of the ϕ as a scalar or pseudoscalar should be possible[3]. The background to this identification is the process $e^+e^- \to ZZ$ which is a t-channel process and thus strongly peaked in large and small θ. The three angular distributions are compared in Figure 2.

More information on the couplings is present in the angular distributions of the decay products of the Z boson. The decays of the spin-0 ϕ should provide no angular information and are not considered here. For the Z decay, two more angles are needed to fully describe the process: $\hat\theta$ and $\hat\varphi$ are the angles in the Z rest frame between the fermion and the Z boost directions.

The differential cross section for the process $e^+e^- \to Z\phi$, $Z \to f\bar f$ is

$$\frac{d\sigma\left(\tau,\tau'\right)}{d\cos\theta\, d\cos\hat\theta\, d\hat\varphi} = \frac{1}{32\pi s}\bar\beta\left(\frac{m_Z^2}{s},\frac{m_\phi^2}{s}\right)\frac{3\mathrm{B}(Z\to f\bar f)}{16\pi}\frac{(v_f+\tau' a_f)^2}{2(v_f^2+a_f^2)}\left|\mathcal{M}_\tau^{\tau'}\right|^2 \tag{2}$$

for a given electron helicity τ and final fermion helicity τ'. We can expand the squared matrix element above in terms of nine independent decay angular distributions:

$$\begin{aligned}\left|\mathcal{M}_\tau^{\tau'}\right|^2 = \quad & \mathcal{F}_1(1+\cos^2\hat\theta)+\mathcal{F}_2(1-3\cos^2\hat\theta)+\mathcal{F}_3\cos\hat\theta \\ & +\mathcal{F}_4\sin\hat\theta\cos\hat\varphi+\mathcal{F}_5\sin(2\hat\theta)\cos\hat\varphi+\mathcal{F}_6\sin^2\hat\theta\cos(2\hat\varphi) \\ & +\mathcal{F}_7\sin\hat\theta\sin\hat\varphi+\mathcal{F}_8\sin(2\hat\theta)\sin\hat\varphi+\mathcal{F}_9\sin^2\hat\theta\sin(2\hat\varphi).\end{aligned} \tag{3}$$

The distributions are defined such that only the coefficient $\mathcal{F}_1$ remains after integration over the decay angles $\hat\theta$ and $\hat\varphi$.

The coefficients $\mathcal{F}_i$ may be expressed compactly in terms of the couplings a_Z and b_Z:

$$\begin{array}{llll}\mathcal{F}_1 = & 4C(1+\cos^2\theta)(sa_Z^2+4p_Z^2s^2b_Z^2)+ & 8C & \sin^2\theta e_Z^2 sa_Z^2/M_Z^2, \\ \mathcal{F}_2 = & 8C\sin^2\theta e_Z^2 sa_Z^2/M_Z^2, & \mathcal{F}_3 = & 16C\tau\cos\theta(sa_Z^2+4p_Z^2s^2b_Z^2), \\ \mathcal{F}_4 = & 16C\tau\tau'\sin\theta E_Z sa_Z^2/M_Z, & \mathcal{F}_5 = & 8C\sin\theta\cos\theta E_Z sa_Z^2/M_Z, \\ \mathcal{F}_6 = & 4C\sin^2\theta(sa_Z^2-4p_Z^2s^2b_Z^2), & \mathcal{F}_7 = & 32C\tau\tau'\sin\theta p_Z E_Z s\sqrt{s}a_Zb_Z/M_Z^2, \\ \mathcal{F}_8 = & 16C\sin\theta\cos\theta p_Z E_Z s\sqrt{s}a_Zb_Z/M_Z^2, & \mathcal{F}_9 = & 16C\sin^2\theta p_Z s\sqrt{s}a_Zb_Z.\end{array}$$

The constant $C = g_Z^2(v_e+\tau a_e)^2/((s-M_Z^2)^2+M_Z^2\Gamma_Z^2)$ and E_Z, p_Z are the energy and momentum of the decaying Z in the lab. This result is less than completely general. In the case that $\phi Z\gamma$ interactions are included in the effective lagrangian, there are more nonzero terms[4]. In particular, there are CP-violating terms in $\mathcal{F}_{1,3,4,5}$. Including the $\phi Z\gamma$ couplings likewise gives CP-conserving contributions to $\mathcal{F}_{7,8}$, but not to $\mathcal{F}_9$, making this the most interesting of the angular distribution terms.

We proceed to form asymmetries which isolate the terms above. First, we integrate out θ, either simply or using a forward-backward asymmetry:

$$f_i = \int_{-1}^{1} d\cos\theta \mathcal{F}_i, \qquad f_i^{\rm FB} = \left(\int_0^1 - \int_{-1}^0\right) d\cos\theta \mathcal{F}_i, \tag{4}$$

then define integrated asymmetries

$$A_i^{(\rm FB)}(\tau) = \frac{1}{N}\sum_f \sum_{\tau,\tau'} \frac{3B(Z\to f\bar{f})}{16\pi}\frac{(v_f+\tau' a_f)^2}{2(v_f^2+a_f^2)} f_i^{(\rm FB)}(\tau,\tau'), \tag{5}$$

$$\sigma_{tot} = \frac{1}{32\pi s}\bar{\beta}(\frac{m_Z^2}{s},\frac{m_\phi^2}{s})N. \tag{6}$$

These asymmetries are listed in Table 1. In addition, we indicate which of these asymmetries will be suppressed without beam polarization or final spin information, and which require identification of the charge of the final fermion f to be observable. Figure 3 shows the values of the asymmetry A_9 for a small coupling b_Z in addition to the standard coupling a_Z.

Fig. 3. CP-violating asymmetry A_9 (see Eq. (5)) for $(\sqrt{s}, m_H)$ = (200,60) GeV (solid) and (300,150) GeV (dotdashed). The curves show the dependence on b_Z; when this coupling is zero, the asymmetry is also zero.

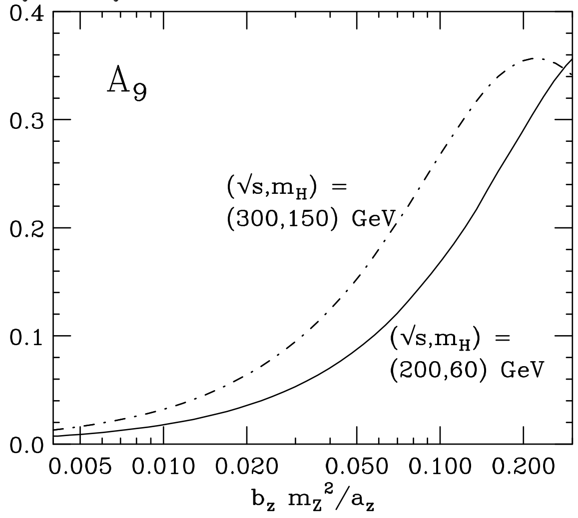

Table. 1. CP properties of the asymmetries. CP (non)conservation is indicated with a (−)+. The circles indicate that the charge of the fermion f must be identified, and the triangles suppression without polarization measurements.

Asym.	CP	beam Pol.	f Pol.	f charge
σ_{tot}	+	-	-	-
A_2	+	-	-	-
A_4	+	△	△	○
$A_5^{\rm FB}$	+	-	-	-
A_6	+	-	-	-
A_7	−	△	△	○
$A_8^{\rm FB}$	−	-	-	-
A_9	−	-	-	-

It is clear that addition of $\phi Z\gamma$ couplings to the effective lagrangian would produce similar effects in the reaction $e^+e^- \to \phi\gamma$. Here the Standard Model tree-level coupling does not exist, so that the small higher-dimension operators would have a more significant effect, that is, interference effects might be much larger. On the other hand, the Standard Model contribution to this process is tiny[11,12,13] and distributions in the scattering angle will be more difficult to measure.

3. Higgs Decays to Vector Bosons

The decay of Higgs to vector boson pairs provides tests of the Higgs parity. The couplings have the same forms in this case as for the associated production discussed above. In particular, the CP-even boson decays to a mixture of longitudinal and transverse polarization, and the CP-odd Higgs to purely transversally polarized bosons. The azimuthal angle φ between the vector boson decay planes may be used to form distributions[14,15,16] $d\Gamma(H \to VV)/d\varphi \propto 1 + a_1 \cos\varphi + a_2 \cos(2\varphi)$, $d\Gamma(A \to VV)/d\varphi \propto 1 - \cos\varphi/4$. Other useful observables are the energies of the fermions in the Higgs rest frame[17,18] and the invariant mass of the off-shell vector boson[3] for the decay $H, A \to VV^*$.

4. $\gamma\gamma$ Production of Higgs Particles

The colliding photon beam reaction $\gamma\gamma \to H, A$ has long been recognized (see e.g. Refs. 7,19) as an important instrument to study the properties of Higgs particles. Using linearly polarized photon beams, the parity of the produced Higgs boson can be measured directly[3,19]. While the polarization vectors of the two photons must be parallel to generate scalar particles, they must be perpendicular for pseudoscalar particles[20],

$$\mathcal{M}(\gamma\gamma \to H) \sim \vec{\epsilon}_1 \cdot \vec{\epsilon}_2, \qquad \mathcal{M}(\gamma\gamma \to A) \sim \vec{\epsilon}_1 \times \vec{\epsilon}_2 \cdot \vec{k}_\gamma \tag{7}$$

High-energy colliding beams of linearly polarized photons can be generated by Compton back-scattering of linearly polarized laser light on electron/positron bunches of e^+e^- linear colliders[21]. The linear polarization transfer from the laser photons to the high-energy photons is described by the ξ_3 component of the Stokes vector. The length of this vector depends on the final state photon energy and on the value of the parameter $x_0 = 4E_e\omega_0/m_e^2$, where E_e and ω_0 are the electron and laser energies. The linear polarization transfer is large for small values of x_0 if the photon energy $y = E_\gamma/E_e$ is close to its maximum value. The maximum value of the Stokes vector $\xi_3(y)$ is reached for $y = y_{\max}$, and approaches unity for small values of x_0[22].

Since only part of the laser polarization is transferred to the high-energy photon beam, it is useful to define the polarization asymmetry $\mathcal{A}$ as

$$\mathcal{A} = \frac{N^{||} - N^{\perp}}{N^{||} + N^{\perp}}, \tag{8}$$

where $N^{\parallel}$ and $N^{\perp}$ denote the number of $\gamma\gamma$ events with the initial laser polarizations being parallel and perpendicular, respectively. It follows from Eq. (8) that

$$\mathcal{A}(\gamma\gamma \to H) = +\mathcal{A}, \qquad \mathcal{A}(\gamma\gamma \to A) = -\mathcal{A} \tag{9}$$

The maximum sensitivity $\mathcal{A}_{\max}$ is reached for small values of x_0 and near the upper bound of $\tau = M_H^2/s_{e^+e^-}$, i. e. if the energy is just sufficient to produce the Higgs particles. Since the luminosity vanishes at $\tau = \tau_{\max}$, the operating conditions must in practice be set such that a sufficiently large luminosity is possible. Typical energies for electron and laser beams are shown in Table 2 for a sample of x_0 values corresponding to large and small asymmetries $\mathcal{A}_{\max}$.

Table 2. Electron (E_e) and laser γ energies (ω_0) for a sample of Higgs masses if the parameter $x_0 = 4E_e\omega_0/m_e^2$, which determines the maximum asymmetry $\mathcal{A}_{\max}$ at $\sqrt{\tau_{\max}} = y_{\max}$, is varied from small to large values.

x_0	$\mathcal{A}_{\max}$	$\sqrt{\tau_{\max}}$	M_H [GeV]	E_e [GeV] (at $\sqrt{\tau_{\max}}$)	ω_0 [eV]
0.5	0.85	0.33	100	150	0.22
			200	300	0.11
			300	450	0.07
1.0	0.64	0.5	100	100	0.65
			200	200	0.33
			300	300	0.22
2.0	0.36	0.67	100	75	1.74
			200	150	0.87
			300	225	0.58
4.83	0.11	0.83	100	60.4	5.22
			200	121	2.61
			300	181	1.74

The measurement of the Higgs parity in $\gamma\gamma$ collisions will be a unique method in areas of the parameter space where the Higgs coupling to heavy W, Z bosons are small and the top quark decay channels are closed so that the Higgs particles decay preferentially to b and c quarks. It must therefore be shown that the background events from heavy quark production can be suppressed sufficiently well. This is a difficult task[7,23] for b quarks. Three components contribute to the $b\bar{b}$ background events: direct $\gamma\gamma$ production, the once-resolved photon process $\gamma\gamma(\to \gamma g) \to b\bar{b}$, and the twice-resolved photon process $\gamma\gamma(\to gg) \to b\bar{b}$ [7,23,24].

The cross section for $\gamma\gamma \to b\bar{b}$ can be easily calculated at the tree level for linearly-polarized photons. Effects due to higher-order QCD corrections have been shown to be modest in the unpolarized case[24] and, hence, can be safely neglected for asymmetries.

The cross sections at energies sufficiently above the quark threshold are given by

$$\frac{d\sigma^{\|}}{dy} = \frac{d\sigma^{\perp}}{dy} = \frac{12\pi\alpha^2 Q_b^4}{s} \frac{1+e^{-4y}}{(1+e^{-2y})^2}, \tag{10}$$

where y denotes the b-quark rapidity. As evident from Eq. (10), the background process $\gamma\gamma \to b\bar{b}$ does not affect the numerator of the asymmetry $\mathcal{A}$, yet it does increase the denominator, thus diluting the asymmetry in general by a significant amount. While the signal events are distributed isotropically in their center-of-mass frame, the background events are strongly peaked at zero polar angles. This can be exploited to reject the background events. In Fig. 4 we compare the (unpolarized) signal cross sections in the Standard Model with the background $b\bar{b}$ channels.

Fig. 4. Signal and background cross sections for $b\bar{b}$ final states in the Standard Model. Here and the subsequent figures, $m_t = 150$ GeV.

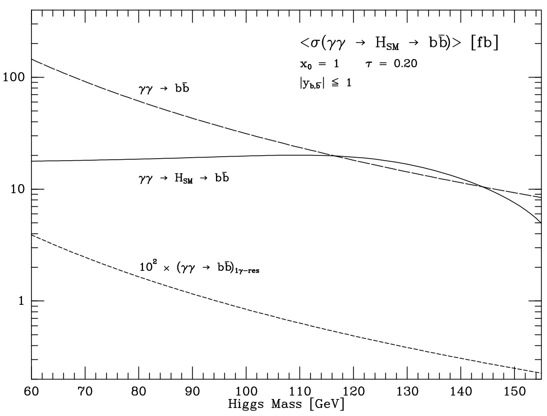

Fig. 5. The polarization asymmetry $\mathcal{A}$ for Standard Model Higgs production including the background process.

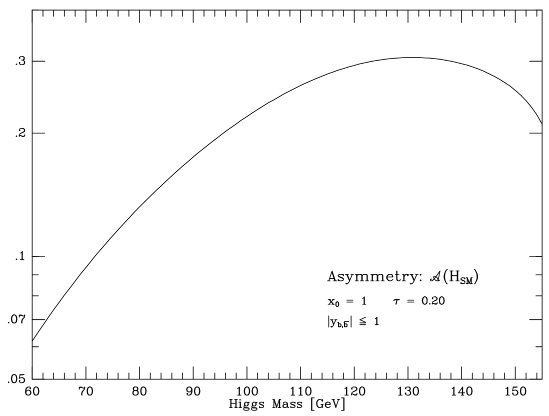

If one or two photons are resolved into quark-plus-gluon showers, the subprocesses $\gamma g \to b\bar{b}$ and $gg \to b\bar{b}$ generate b-quark final states. Since gluons are generated only in the double-splitting process $\gamma \to q \to g$, the gluon spectrum falls off steeply with gluon momentum. Therefore, the once- and twice-resolved processes are strongly suppressed if nearly all the photon energy is needed to generate the $b\bar{b}$ final state energy. This is the situation we encounter for τ values close to $\tau_{\max}(x_0)$, that is, for large asymmetries $\mathcal{A}$. The background from once-resolved processes is thus small in this kinematical configuration and negligible for the twice-resolved process.

It is clear from the figures that the measurement of the Higgs parity, in particular for the heavy particles, requires high $\gamma\gamma$ luminosities. The background events reduce the asymmetry $\mathcal{A}$ by a factor $1/[1+B/S]$ where S (B) denote the number of signal (background) events. The asymmetries including background events are displayed in

Figs. 5–7 for the Standard Model Higgs particle H_{SM} and for the h^0/A^0 particles in the minimal supersymmetric model.

The polarization asymmetry of the $\mathcal{SM}$ Higgs particle H_{SM} can be measured in $\gamma\gamma$ collisions throughout the relevant mass range below $\sim$ 150 GeV in the $b\bar{b}$ channel; above this mass value Higgs decays to Z bosons can be exploited to determine spin and parity. The light scalar $\mathcal{MSSM}$ Higgs boson h^0 can be probed in a similarly comprehensive way, except presumably for the low mass range at large $\tan\beta$. Finally, the $\gamma\gamma$ polarization measurement of the parity in the very interesting case of the pseudoscalar A^0 Higgs particle appears feasible throughout most of the parameter range below the top threshold; $A^0 \to t\bar{t}$ decays can be exploited for masses above this threshold.

Fig. 6. The polarization asymmetry $\mathcal{A}$ for SUSY h^0 production including the background process.

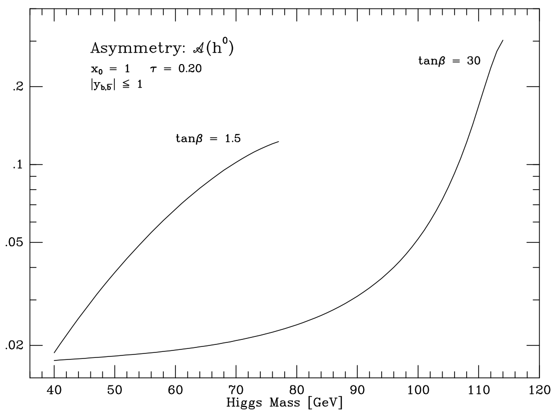

Fig. 7. The polarization asymmetry $\mathcal{A}$ for SUSY A^0 production, including background.

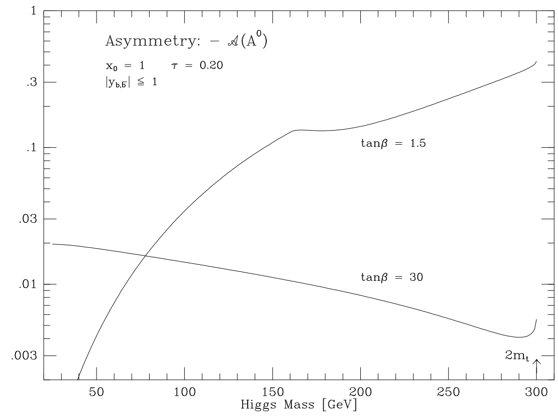

5. Neutral Higgs Decays to Fermion Pairs

The coupling of neutral Higgs particles to fermion pairs also provides tests of the Higgs parity. Two conditions on the useful decay modes exist here. The first, that it be a mode with relatively high branching fraction, is satisfied for the $b\bar{b}$ mode and also for $\tau^+\tau^-$ and perhaps for $t\bar{t}$. The b decay channel is in general the most frequent decay mode in the Standard Model[25,26] as well as in its minimal supersymmetric extension[27]. Much cleaner channels, though with branching ratios suppressed by an order of magnitude, are the τ and t modes. The τ channel is useful in the $\mathcal{SM}$ for Higgs masses less than $\sim$ 130 GeV and in supersymmetric theories generally over a much larger mass range[27]. Top quark decays are of interest in a wide range above the top threshold[28].

The second requirement, that the spin of the fermion be experimentally observable, is satisfied at present only for the τ and t decay modes. Due to the depolarization effects in the fragmentation process, it is very difficult to extract information on the b polarization state[29]. For large top masses, the top quarks decay before fragmentation destroys the t-spin information[30].

Denoting the spin vectors of the fermion f and the antifermion $\bar{f}$ in their respective rest frames by s and $\bar{s}$, with the $\hat{z}$-axis oriented in the f flight direction, the spin dependence of the decay probability is given by[3]

$$\Gamma(H, A \to f\bar{f}) \quad \propto \quad 1 - s_z \bar{s}_z \pm s_\perp \bar{s}_\perp \tag{11}$$

This spin dependence translates directly into correlations among the fermion decay products.

Although the decay mode $\tau^\pm \to \pi^\pm \nu_\tau(\overline{\nu}_\tau)$ is rare, it serves as a simple example. Defining the polar angles between the $\pi^\pm$ and the τ^- direction in the $\tau^\pm$ rest frames by $\hat{\theta}_\pm$ and the relative azimuthal angle $\hat{\varphi}$ between the decay planes, the angular correlation may be written

$$\frac{1}{\Gamma} \frac{d\Gamma(H, A \to \pi^+ \overline{\nu} \pi^- \nu)}{d\cos\hat{\theta}_+ d\cos\hat{\theta}_- d\hat{\varphi}} \quad = \quad \frac{1}{8\pi} \left[1 + \cos\hat{\theta}_- \cos\hat{\theta}_+ \mp \sin\hat{\theta}_+ \sin\hat{\theta}_- \cos\hat{\varphi}\right]. \tag{12}$$

The full sensitivity to the Higgs parity, reflected in the equal coefficients of the constant and spin-dependent terms in Eq. (11), is retained in this case. This is a consequence of the spin-0 nature of the pion.

A useful observable sensitive to the parity of the decaying Higgs particle is the angle δ between the two charged pions in the Higgs rest frame[31]. Although the resulting distributions are very similar for most values of δ, they behave differently in the limit $\delta \to \pi$. The scalar distribution approaches its maximum at $\delta = \pi$, while the pseudoscalar distribution peaks at a small but nonzero value of $\pi - \delta$. In the limit of vanishing pion mass, the distribution approaches zero as the pions are emitted back-to-back. Since the pion mass is very much smaller than the τ mass, the distributions for non–zero pion masses have much the same behavior in the limit of back-to-back pions.

Other τ decay modes also provide the opportunity to extract the Higgs parity. Let us consider the case of both τ's decaying to $\rho(\hat{=}2\pi)$. As the ρ is a spin-1 particle, the correlation term in Eq. (12), and hence the sensitivity of the process to the Higgs parity, is reduced by the factor $(m_\tau^2 - 2Q^2)^2/(m_\tau^2 + 2Q^2)^2$. Predictions for the distribution of the acollinearity are shown in Fig. 8 for fixed $Q^2 = m_\rho^2$. The suppression factor is even more severe in the three-pion channel, where $Q^2 \approx m_\tau^2/2$.

These suppression factors can be avoided in the case that an event-by-event reconstruction of the τ decays is possible. In the $\tau \to \pi\nu$ decay, the direction of the pion momentum (defined in the τ rest frame) appears in Eq. (12), replacing the spin vector $\vec{s}$ of Eq. (11). In the general case, $s(\bar{s})$ must be replaced by the vector $\pm R^\mp/(m_\tau \omega_\mp)$, where R and ω are defined by[31]

$$\begin{aligned}
\Pi_\mu &= 4\Re J_\mu q\cdot J^* - 2q_\mu J\cdot J^* \\
\Pi_{5\mu} &= 2\epsilon_{\mu\nu\rho\sigma}\Im J^\rho J^{*\nu} q^\sigma \\
\omega &= p_\mu(\Pi^\mu - \gamma_{\rm AV}\Pi_5^\mu) \\
R_\mu &= (m_\tau^2 g_{\mu\nu} - p_\mu p_\nu)(\gamma_{\rm AV}\Pi^\nu - \Pi_5^\nu)
\end{aligned} \tag{13}$$

q is the momentum of the neutrino, $p_\pm$ is the momentum of the $\tau^\pm$ and $J_\pm$ is the hadronic current, and $\gamma_{\rm AV} = 2g_{\rm A}g_{\rm V}/(g_{\rm A}^2 + g_{\rm V}^2)$. If the τ rest frame is reconstructed, for example with the help of microvertex detectors, then $\vec{R}/(m_\tau\omega)$ can be evaluated in this frame. Since $R_\mu R^\mu/(m_\tau\omega)^2 = -1$, the sensitivity is completely retained.

For the example of the τ decay to $\rho \to 2\pi$, the simple distribution in the hadronic momentum gave a reduced sensitivity to the Higgs parity. In this case, the optimal direction for the angular reconstruction[32] is that of the vector $\vec{R} \propto m_\tau(\vec{\pi}^- - \vec{\pi}^0)(E_{\pi^-} - E_{\pi^0}) + (\vec{\pi}^- + \vec{\pi}^0)m_\rho^2/2$. The angles $\hat{\theta}_\pm$ and $\hat{\varphi}$ are then those defining the direction of $\vec{R}$ in the τ rest frame, and the angular distribution has the form of Eq. (12).

Fig. 8. Distributions of the decay $H, A \to \tau^+\tau^- \to h^+\overline{\nu}_\tau h^-\nu_\tau$ in the angle between the hadrons $h = \pi$, ρ for $M_{H,A} = 150$ GeV. The distributions for scalar (pseudoscalar) Higgs particles are drawn with solid (dashed) lines.

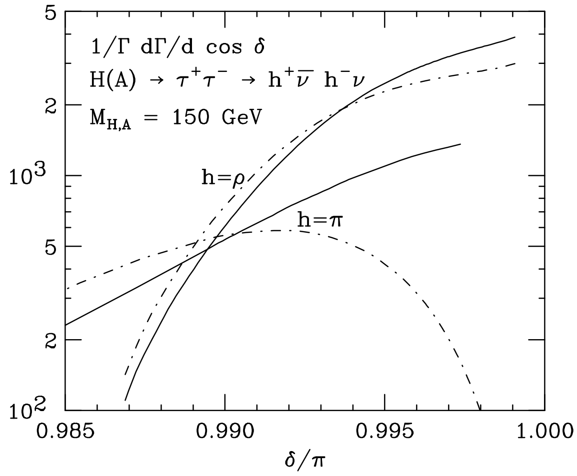

Fig. 9. Distributions of the decays $H, A \to t\bar{t} \to (bl^+\nu)(\bar{b}l^-\overline{\nu})$ in the angle between the charged leptons. Scalar (solid) and pseudoscalar (dashed) distributions are shown for $m_t = 150$ GeV and $m_{H,A} = 400, 1000$ GeV.

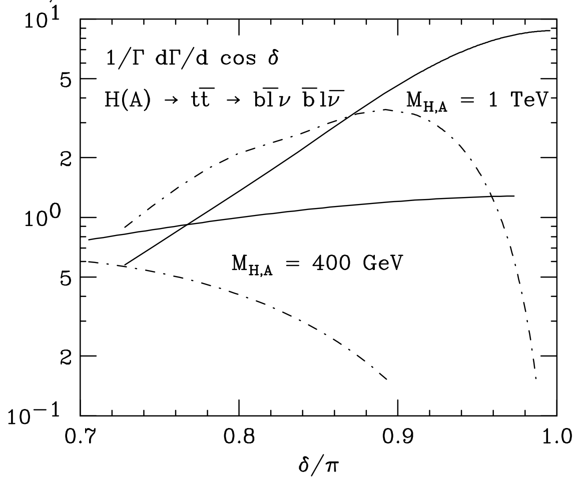

The decay $H, A \to t\bar{t} \to (bW^+)(\bar{b}W^-)$ can be treated in direct analogy to the τ decay to ρ. In this case, the suppression factor $[(m_t^2 - 2M_W^2)/(m_t^2 + 2M_W^2)]^2 \simeq 0.17$. A particularly interesting process is provided by subsequent decays of the $W^\pm$ bosons to leptons. In this case the top quark direction can be reconstructed completely. The distribution obtained after integration over the b-quark directions is exactly the same as in Eq. (12) with the angles $\hat{\theta}_{\pm}$ denoting now the polar angles between the leptons and the top quarks in the quark rest frames. Furthermore, the difference between scalar and pseudoscalar distributions is visible over a much larger angular range, as the Higgs–to–top boosts are generally small, see Fig. 9.

6. Conclusions

The analyses in the preceding sections provide a picture of prospects to determine experimentally the external quantum numbers J^{PC} of scalar (H) and pseudoscalar (A) Higgs particles.

The production of Higgs and Z boson in e^+e^- reactions is interesting for tests of parity and of CP violation in the Higgs sector. The coupling of pseudoscalar Higgs to vector bosons is however generally not present at tree level, so that the sensitivity of this process is small for A^0. The situation is analogous for Higgs decay to two vector bosons.

The decay of Higgs to fermion pairs provides angular correlations sensitive to the Higgs parity for those fermions for which spin information is experimentally available, the τ lepton and, for sufficiently heavy Higgs, the top quark.

The collision of linearly-polarized photon beams is particularly interesting for tests of the Higgs parity. The coupling of both scalar and pseudoscalar Higgs to two photons occurs first at one-loop level, so that the sensitivity of this process to both types of states is similar.

7. Acknowledgements

I would like to thank K. Hagiwara, M. Krämer, J. Kühn, and P. Zerwas for collaborations on the topics discussed in this work.

8. References

1. P. W. Higgs, *Phys. Rev. Lett.* **12** (1964) 132 and *Phys. Rev.* **145** (1966) 1156; F. Englert and R. Brout, *Phys. Rev. Lett.* **13** (1964) 321; G. S. Guralnik, C. R. Hagen and T. Kibble, *Phys. Rev. Lett.* **13** (1964) 585.
2. J. F. Gunion and H. E. Haber, *Nucl. Phys.* **B272** (1986) 1 and **B278** (1986) 449.
3. V. Barger, K. Cheung, A. Djouadi, B. A. Kniehl, and P. M. Zerwas, *Phys. Rev.* **D49** (1994) 79.
4. K. Hagiwara and M. L. Stong, *Z. Phys.* **C62** (1994) 99.
5. J. R. Dell' Aquila and C. A. Nelson, *Nucl. Phys.* **B320** (1989) 61.
6. J. R. Dell' Aquila and C. A. Nelson, *Nucl. Phys.* **B320** (1989) 89.
7. J. F. Gunion and H. E. Haber, *Phys. Rev.* **D48** (1993) 5109.

8. W. Buchmüller and D. Wyler, *Nucl. Phys.* **B268** (1986) 621.
9. K. Hagiwara, S. Ishihara, R. Szalapski and D. Zeppenfeld, *Phys. Lett.* **B283** (1992) 353; *Phys. Rev.* **D48** (1993) 2182.
10. K. Hagiwara, R. D. Peccei, D. Zeppenfeld and K. Hikasa, *Nucl. Phys.* **B282** (1987) 253.
11. R. N. Cahn, M. S. Chanowitz, and N. Fleishon, *Phys. Lett.* **82B** (1979) 113.
12. L. Bergstrom and G. Hulth, *Nucl. Phys.* **B259** (1985) 137.
13. A. Barroso, J. Pulido, and J. C. Romão, *Nucl. Phys.* **B267** (1986) 509.
14. A. Djouadi and B. Kniehl, *Proceedings of the Workshop on e^+e^- Collisions*, Munich-Annecy-Hamburg Nov. 20, 1992 – Apr. 3, 1933.
15. C. A. Nelson, *Phys. Rev.* **D37** (1988) 1220.
16. D. Chang and W.-Y. Keung, *Phys. Lett.* **B305** (1993) 261.
17. A. Skjold and P. Osland, *Phys. Lett.* **B311** (1993) 261, and *Phys. Lett.* **B329** (1994) 305.
18. T. Arens and L. M. Sehgal, Preprint PITHA-94-37 (hep-ph 9409396), and T. Arens, U. D. J. Gieseler and L. M. Sehgal, *Phys. Lett.* **B339** (1994) 127.
19. B. Grządkowski and J. F. Gunion, *Phys. Lett.* **B294** (1992) 361.
20. C. N. Yang, *Phys. Rev.* **77** (1949) 242.
21. I. F. Ginzburg, G. L. Kotkin, S. L. Panfil, V. G. Serbo, and V. I. Telnov, *Nucl. Instr. and Meth.* **219** (1984) 5.
22. M. Krämer, J. Kühn, M. L. Stong, and P. M. Zerwas, *Z. Phys.* **C64** (1994) 21.
23. O. J. P. Eboli, M. C. Gonzales-Garcia, F. Halzen and D. Zeppenfeld, *Phys. Rev.* **D48** (1993) 1430.
24. M. Drees, M. Krämer, J. Zunft and P. M. Zerwas, *Phys. Lett.* **B306** (1993) 371; J. H. Kühn, E. Mirkes and J. Steegborn, *Z. Phys.* **C57** (1993) 615.
25. A. Djouadi, D. Haidt and P. M. Zerwas, *Proceedings, "e^+e^- Colliders at 500 GeV: The Physics Potential"*, DESY 92-123A; R. Kleiss, Z. Kunszt and W. J. Stirling, *Phys. Lett.* **B253** (1991) 269.
26. B. A. Kniehl, *Phys. Rep.* **240** (1994) 211.
27. A. Djouadi, J. Kalinowski and P. M. Zerwas, *Proceedings, "e^+e^- Colliders at 500 GeV: ThePhysics Potential"*; *Z. Phys.* **C57** (1993) 569.
28. K. Hagiwara, H. Murayama and I. Watanabe, *Nucl. Phys.* **367** (1991) 257; H. Veltman, *Z. Phys.* **C62** (1994) 235.
29. B. Mele and G. Altarelli, *Phys. Lett.* **B299** (1993) 345; B. Mele, *Proceedings, XXVII Recontres de Moriond*, Les Arcs 1992.
30. J. H. Kühn, *Acta Phys. Aus. Suppl.* **24** (1982) 203; I. I. Y. Bigi, Y. L. Dokshitser, V. Khoze, J. H. Kühn and P. M. Zerwas, *Phys. Lett.* **181B** (1986) 157.
31. J. H. Kühn and F. Wagner, *Nucl. Phys.* **B236** (1984) 16.
32. B. Grządkowski and J. F. Gunion, Preprint UCD-95-5 (hep-ph 9501339).